

Involvement of Receptor Activator of Nuclear Factor- κ B Ligand (RANKL)-induced Incomplete Cytokinesis in the Polyploidization of Osteoclasts^{*[S]}

Received for publication, July 6, 2015, and in revised form, November 23, 2015. Published, JBC Papers in Press, December 15, 2015, DOI 10.1074/jbc.M115.677427

Noriko Takegahara^{‡S1}, Hyunsoo Kim[§], Hiroki Mizuno^{¶||}, Asako Sakaue-Sawano^{**}, Atsushi Miyawaki^{**}, Michio Tomura^{‡‡S5}, Osami Kanagawa^{¶||}, Masaru Ishii^{¶||}, and Yongwon Choi^{‡S2}

From the [‡]Next Generation Optical Immune-imaging, WPI-Immunology Frontier Research Center, Osaka University, Suita, Osaka 565-0871, Japan, the [§]Department of Pathology and Laboratory Medicine, University of Pennsylvania Perelman School of Medicine, Philadelphia, Pennsylvania 19104, the [¶]Department of Immunology and Cell Biology, Graduate School of Medicine and Frontier Biosciences, WPI-Immunology Frontier Research Center, Osaka University, 2-2 Yamada-oka, Suita, Osaka 565-0871, Japan, the ^{||}CREST, Japan Science and Technology Agency, 5 Sanban-cho, Chiyoda-ku, Tokyo 102-0075, Japan, the ^{**}Laboratory for Cell Function and Dynamics, Advanced Technology Development Group, Brain Science Institute, RIKEN, Wako-city, Saitama 351-0198, Japan, the ^{‡‡}Laboratory for Autoimmune Regulation, Research Center for Allergy and Immunology, RIKEN, Yokohama City, Kanagawa 230-0045, Japan, the ^{S5}Laboratory of Immunology, Faculty of Pharmacy, Osaka-Ohtani University, 3-11-1 Nishikiorikita, Tondabayashi-city, Osaka 584-8540, Japan, and the ^{¶¶}Department of Molecular Preventive Medicine, Graduate School of Medicine, University of Tokyo, 7-3-1 Hongo, Bunkyo-ku, Tokyo 113-033, Japan

Osteoclasts are specialized polyploid cells that resorb bone. Upon stimulation with receptor activator of nuclear factor- κ B ligand (RANKL), myeloid precursors commit to becoming polyploid, largely via cell fusion. Polyploidization of osteoclasts is necessary for their bone-resorbing activity, but the mechanisms by which polyploidization is controlled remain to be determined. Here, we demonstrated that in addition to cell fusion, incomplete cytokinesis also plays a role in osteoclast polyploidization. In *in vitro* cultured osteoclasts derived from mice expressing the fluorescent ubiquitin-based cell cycle indicator (Fucci), RANKL induced polyploidy by incomplete cytokinesis as well as cell fusion. Polyploid cells generated by incomplete cytokinesis had the potential to subsequently undergo cell fusion. Nuclear polyploidy was also observed in osteoclasts *in vivo*, suggesting the involvement of incomplete cytokinesis in physiological polyploidization. Furthermore, RANKL-induced incomplete cytokinesis was reduced by inhibition of Akt, resulting in impaired multinucleated osteoclast formation. Taken together, these results reveal that RANKL-induced incomplete cytokinesis contributes to polyploidization of osteoclasts via Akt activation.

Polyploidy, in which a cell has more than the diploid complement of chromosomes, is a widespread physiological phenom-

enon observed especially in plants, fungi, and insects (1). Although it is less common in mammals, polyploidization occurs in selected tissues, including the placenta, liver, heart, skeletal muscle, and bone marrow during normal development and aging (2). During developmental programs, cells obtain additional sets of chromosomes by various mechanisms, including endocycles, endomitosis, incomplete cytokinesis, and cell fusion. In endocycles and endomitosis, the cell undergoes successive rounds of DNA replication without intervening mitosis or karyokinesis (abort mitosis during metaphase). These cycles do not produce two nuclei in the cell. The best-studied examples of endocycles and endomitosis are trophoblast giant cells and megakaryocytes, respectively (3–6). In incomplete cytokinesis, the cell undergoes karyokinesis but skips cytokinesis, resulting in a cell with two nuclei; this process has been implicated in the normal development of hepatocytes and cardiomyocytes (7, 8). Cell fusion, which involves merging of the plasma membrane and cytoplasmic mixing, is observed during development of skeletal muscle cells and osteoclasts (9, 10). Endocycles, endomitosis, and incomplete cytokinesis are directly associated with the proliferative state of the cell. By contrast, cell fusion is entirely independent of cell proliferation (10).

Polyploidy is a hallmark of mature osteoclasts, which are specialized multinucleated giant cells that resorb bone (11). These cells are hematopoietic in origin and are derived from myeloid precursors that also give rise to macrophages and dendritic cells. When myeloid precursors receive signals mediated by the osteoclast differentiation factor RANKL,³ which is mainly produced by osteoblasts, they commit to becoming pre-osteoclasts and ultimately differentiate into multinucleated osteoclasts (12). The importance of polyploidization in osteoclast forma-

* This work was supported by the Uehara Memorial Foundation, the Nakatomi Foundation, Tomizawa Jun-ichi and Keiko Fund of the Molecular Biology Society of Japan for Young Scientists, the Pharma-link between Academia and Shionogi, the Takeda Science Foundation (to N.T.), and in part by National Institutes of Health Grants AR055903 and AR067726 (to Y.C.). The authors declare that they have no conflicts of interest with the contents of this article. The content is solely the responsibility of the authors and does not necessarily represent the official views of the National Institutes of Health.

Author's Choice—Final version free via Creative Commons CC-BY license.

[S] This article contains supplemental Movies S1–S5.

¹ To whom correspondence may be addressed: Osaka University, Suita, Osaka 565-0871, Japan. Tel.: 81-06-6879-3881; Fax: 81-06-6879-3889; E-mail: takegaharanor@gmail.com.

² To whom correspondence may be addressed. Tel.: 215-746-6404; Fax: 215-573-0888; E-mail: ychoi3@mail.med.upenn.edu.

³ The abbreviations used are: RANKL, receptor activator of nuclear factor- κ B ligand; MGC, multinucleated giant cell; BMM, bone marrow-derived macrophage; dTg, double-transgenic; 7-AAD, 7-aminoactinomycin; BP, band path filter; mAG, monomeric Azami Green.

Osteoclast Polyploidization via Incomplete Cytokinesis

tion is demonstrated by the impaired bone-resorbing activity of osteoclasts that cannot achieve polyploidy (13).

Although generation of polyploid osteoclasts is thought to occur due to cell fusion, independently of cell proliferation (14), some researchers have pointed out a relationship between cell proliferation and osteoclast differentiation. For example, in osteoclast progenitors, progression and subsequent withdrawal from the cell cycle are required for differentiation into osteoclasts (15–17). In addition, stimulation with RANKL also triggers a signaling pathway that is essential for cell cycle progression (18). These reports prompted us to investigate whether cell cycle progression has an impact on polyploidization during osteoclastogenesis and, if so, how and to what extent the cell cycle regulates the polyploidization of osteoclasts. The fluorescent ubiquitination-based cell cycle indicator (Fucci) is a powerful tool for studying coordination of the cell cycle with other developmental processes (19–22). The Fucci probe was generated by fusing red fluorescent protein and green fluorescent protein to human Cdt1 and human geminin, respectively. These two chimeric proteins accumulate reciprocally in the nuclei during the cell cycle, labeling the nuclei of cells in G₀/G₁ phase red and those in S/G₂/M phase green. Thus, these proteins function as effective G₀/G₁ and S/G₂/M markers.

Here, using monocytes derived from Fucci transgenic mice, we show that RANKL-induced polyploidization occurs not only by cell fusion but also by incomplete cytokinesis. In these cells, RANKL stimulation transiently increased basal proliferation and induced incomplete cytokinesis as well as cell fusion. Also, cells that underwent incomplete cytokinesis had the potential to undergo cell fusion. In addition, fluorescence *in situ* hybridization revealed that some of osteoclasts exhibited nuclear polyploidy (*i.e.* they contained nuclei with more than the diploid complement of chromosomes (>2N)) *in vivo*, suggesting that cells that undergo incomplete cytokinesis are involved in physiological polyploidization of osteoclasts. Furthermore, RANKL stimulation induced phosphorylation of Akt, which is required for efficient polyploidization by either incomplete cytokinesis or cell fusion. Collectively, our findings reveal an unexpected pattern of cell division and fusion during the generation of polyploid osteoclasts.

Experimental Procedures

Mice—Fucci transgenic mouse lines FucciS/G₂/M-#474 and FucciG₁-#639 were obtained from the RIKEN BioResource Center. These lines were cross-bred to obtain Fucci double-transgenic mice. The generation of TRAP promoter-tdTomato transgenic mice and V-type H⁺-ATPase α 3 subunit-GFP fusion protein expressing mice (α 3-GFP) were described previously (23). All animal work was performed under veterinary supervision in an accredited facility using protocols approved by the Animal Care and Use Committee of the University of Pennsylvania and Osaka University.

In Vitro Osteoclast and Multinucleated Giant Cell Differentiation—Bone marrow-derived macrophages (BMMs) from wild type (WT) or Fucci double-transgenic (dTg) mice were obtained from cultures of bone marrow collected from 6- to 8-week-old male tibias and femurs, as described previously. In brief, bone marrow progenitor cells were cultured with

M-CSF (60 ng/ml) in α -minimal essential medium containing 10% FCS. After 3–4 days, cells were gathered as BMMs. For osteoclast differentiation, BMMs were cultured for 3 days in α -minimal essential medium containing M-CSF (60 ng/ml) and RANKL (150 ng/ml). After culture for 3 days, the cells were fixed with 3.7% formaldehyde in PBS for 10 min and then stained for TRAP using the acid phosphatase, leukocyte (TRAP) kit (Sigma). TRAP-positive multinucleated cells containing three or more nuclei were counted. For differentiation of multinucleated giant cells (MGCs), BMMs derived from wild type mice were cultured in the presence of IL-3 (100 ng/ml) (R&D Systems) and IL-4 (100 ng/ml) (PeproTech) for 2 days. MGCs were stained with May-Grünwald Giemsa stain (Life Technologies, Inc.). For inhibitor assays, BMMs were cultured with M-CSF (60 ng/ml) and RANKL (150 ng/ml) or with IL-4 (100 ng/ml) plus IL-3 (100 ng/ml) in the presence of Y27632 (10 μ M) (Wako), Akt inhibitor VIII (5 μ M) (Sigma), SN50 (50 μ g/ml) (BioVision), LY294003 (5 μ M) (Wako), aphidicolin (500 nM) (Sigma), or DMSO for 72 h.

BrdU Incorporation Assay—Wild Type-BMMs were cultured with M-CSF (60 ng/ml) in the presence or absence of RANKL (150 ng/ml) or cultured with IL-4 (10 ng/ml) plus IL-3 (100 ng/ml) for the indicated amount of time (in hours). BrdU (10 μ M) were added to the culture for the last 6 h. After culture, cells were washed with PBS and detached using enzyme-free cell dissociation buffer (Millipore) at 37 °C for 5 min. After generation of single-cell suspensions, cells were counted and suspended at 1×10^6 /ml in PBS in polystyrene tubes. The cells were stained with LIVE/DEAD Aqua (Life Technologies, Inc.) for 30 min on ice to exclude dead cells. Cells were washed with PBS with 2% FCS and fixed with BrdU fixation buffer (eBioscience) for 1 h on ice followed by DNase treatment. Cells were stained with FITC-labeled anti-BrdU antibody (clone Bu20a, eBioscience) for 20 min, and after washing, cells were further stained with 7-AAD. Finally, the cells were analyzed using a FACSCanto II (BD Biosciences). Numbers indicate the percentages of S phase cells. Results are representative of three independent experiments.

Ploidy Analysis—dTg-BMMs stimulated with RANKL for the indicated times in the presence of M-CSF were washed with PBS and detached using enzyme-free cell dissociation buffer (Millipore) at 37 °C for 5 min. After generation of single-cell suspensions, cells were counted and suspended at 1×10^6 /ml in phenol red-free α -minimal essential medium containing 2% FCS and 2 mM EDTA in polystyrene tubes. Then the cells were stained with 5 μ M Vybrant DyeCycle Violet (Life Technologies, Inc.) at 37 °C for 60 min. Finally, the cells were stained with TO-PRO-3 (Life Technologies, Inc.) to exclude dead cells and analyzed using an LSR (BD Biosciences). Excitation laser lines and emission filters were as follows: Vybrant DyeCycle Violet: excitation, 405-nm laser line, and emission, 450/50 BP; mAG: excitation, 488-nm laser line, and emission, 515/20 BP; mKO2: excitation, 532-nm laser line, and emission, 585/42 BP; TO-PRO-3: excitation, 640-nm laser line, and emission, 660/20 BP. Data were analyzed using the FlowJo software (Tree Star).

Time-lapse Microscopy and Analysis—dTg-BMMs cultured in a glass-bottom dish were stimulated with RANKL (150 ng/ml) in the presence of M-CSF (60 ng/ml) or stimulated with IL-4 (100 ng/ml) and IL-3 (100 ng/ml) for the indicated times,

and then subjected to time lapse imaging. Cell-tracking experiments were performed using a Deltavision microscope (Applied Precision) from an Olympus IX70 microscope equipped with a $\times 20$ or $\times 40$ objective, 300-watt xenon lamp, and a Photometrics CoolSNAP HQ 12-bit monochrome-cooled CCD camera. A series of images was collected every 5 min at 37 °C. To acquire large square fields of view, multipoint time-lapse imaging was performed. Image acquisition and processing were performed using the Deltavision SoftWorx software (Applied Precision), and image analysis was performed using the Fiji software (National Institutes of Health). Cells were manually tracked. Mononucleated cell fusion was counted as “cell fusion.” Mononucleated or binucleated cells that went through cell fusion following incomplete cytokinesis, or daughter cells of a binucleated cell that underwent cell fusion, were counted as “cell fusion involving incomplete cytokinesis.” Doubling times of cytokinesis/incomplete cytokinesis were assessed using a Nikon BioStation IMQ imaging system, and image analysis was performed using the Imaris software (Bitplane). The time from the end of cytokinesis/incomplete cytokinesis to the next end of cytokinesis/incomplete cytokinesis was measured as the doubling time. Final graphs were generated using GraphPad Prism (GraphPad Software).

Flow Cytometry—dTg-BMMs cultured with M-CSF (60 ng/ml) in the presence or absence of RANKL (150 ng/ml) for 48 h were washed with PBS and detached using enzyme-free cell dissociation buffer (Millipore) at 37 °C for 5 min. After generation of single-cell suspensions, cells were counted and suspended at 1×10^6 /ml in PBS in polystyrene tubes. Cells were stained with 1 μ M LIVE/DEAD NearIR (Life Technologies, Inc.) on ice for 30 min to exclude dead cells, washed with PBS with 2% FCS, and stained with allophycocyanin-labeled antibodies against integrin $\beta 3$ or F4/80 (integrin $\beta 3$, clone 2C9.G3; F4/80, clone MB8 (eBioscience)) on ice for 30 min. After washing, cells were further stained with 5 μ M Vybrant DyeCycle Violet (Life Technologies, Inc.) at 37 °C for 60 min. A Fucci transgenic mouse line FucciG1-#610 obtained from the RIKEN BioResource Center and a3-GFP mice line were cross-bred to obtain Fucci-mKO2 and a3-GFP expressing mice (Fucci-mKO2/a3-GFP). BMMs were prepared from Fucci-mKO2/a3-GFP mice and cultured with M-CSF (60 ng/ml) in the presence or absence of RANKL (150 ng/ml) for the indicated times. After generation of single-cell suspensions, cells were stained with 5 μ M Vybrant DyeCycle Violet (Life Technologies, Inc.) at 37 °C for 60 min. Finally, the cells were stained with TO-PRO-3 (Life Technologies, Inc.) to exclude dead cells. Peripheral blood cells or bone marrow cells of Fucci-mAG transgenic mice were stained with allophycocyanin-labeled antibodies against Ly6C (clone HK1.4 (eBioscience)) on ice for 30 min. After washing, cells were further stained with 5 μ M Vybrant DyeCycle Violet (Life Technologies, Inc.) at 37 °C for 60 min. Finally, the cells were stained with 7-AAD (eBioscience) to exclude dead cells. Cells were analyzed using LSR (BD Biosciences), and data were analyzed using the FlowJo software (Tree Star).

Gelatin Degradation Assay—Fluorescein isothiocyanate (FITC) gelatin-coated glass bottom dishes were prepared as described previously (24). dTg-BMMs were cultured on the FITC gelatin-coated dishes for 24 h with M-CSF (60 ng/ml) and

RANKL (150 ng/ml) and then subjected to time-lapse imaging using a confocal A1 microscope system (Nikon). A series of images was collected every 30 min at 37 °C. Image analysis was performed using NIS-elements software (Nikon).

Fluorescence in Situ Hybridization—TRAP promoter-tdTomato transgenic mice were perfused with 4% paraformaldehyde plus sucrose for fixation, and bone tissues were further fixed with 4% paraformaldehyde plus sucrose for 3 h at 4 °C. Next, the bones were incubated with 10% EDTA for 2 weeks for decalcification and embedded in O.C.T. compound (Tissue-Tek). Sections 5 μ m thick were prepared using Kawamoto's film method and treated with pepsin, and then FISH probe mixture was added. The sections were denatured at 90 °C for 10 min and then kept overnight at 37 °C for hybridization. After hybridization, the sections were washed with 5% formamide, $2 \times$ SSC for 20 min at 37 °C, and then $1 \times$ SSC for 10 min at room temperature. After washing, the sections were stained with DAPI, and images were acquired using the Leica CW-4000 system (Leica) with a $\times 100$ objective.

Western Blotting—After treatment of cells with the indicated cytokines or inhibitors for the indicated times, cells were washed twice with ice-cold PBS and scraped from the plastic plate with a cell lifter (Costar), and then whole-cell lysates were isolated in RIPA buffer (1% Nonidet P-40, 0.5% sodium deoxycholate, 0.1% SDS, 25 mM Tris-HCl, pH 7.6, 150 mM NaCl) supplemented with protease inhibitor mixture and PhosSTOP (Roche Applied Science). Equivalent amounts of protein (20–40 μ g) were subjected to 10% SDS-PAGE, and immunoblotting was performed using antibodies specific for phospho-Akt (Ser-473), Akt, phospho-p38 MAPK (Thr-180/Tyr-182), p38, phospho-p44/42 MAPK (ERK1/2) (Thr-202/Tyr-204), ERK1/2, JNK (Cell Signaling), and phospho-JNK (Thr-183/Tyr-185) (BD Biosciences). For RhoA activation assay, cell lysates were incubated with Rhotekin-RBD protein beads and blotted with anti-RhoA mAb (Cytoskeleton).

Statistical Analysis—Data were analyzed using one-way analysis of variance or unpaired *t* test with Welch's correction and are presented as means \pm S.D. A *p* value < 0.05 was considered significant.

Results

RANKL Stimulation Increases Basal Proliferation of BMMs—To determine the impact of RANKL stimulation on the cell cycle during osteoclast development, we first examined the proportions of cells in the G_1 and $S/G_2/M$ phases during RANKL-induced osteoclast differentiation. Fucci double-transgenic mouse-derived bone marrow monocytes (dTg-BMMs) were stimulated with or without RANKL in the presence of M-CSF, and the proportions of the cells positive for green fluorescence ($S/G_2/M$ phase) and red fluorescence (G_1 phase) were measured by flow cytometry. The proportion of green cells increased 24 h after RANKL stimulation, but this increase disappeared 48 h after stimulation (Fig. 1, A and B). M-CSF alone did not significantly influence the proportion of green or red cells during this period (Fig. 1, A and B). These results suggested that RANKL stimulation transiently promotes cell cycle progression. The increase in cell cycle progression was confirmed by BrdU incorporation assay (Fig. 1C).

Osteoclast Polyplodization via Incomplete Cytokinesis

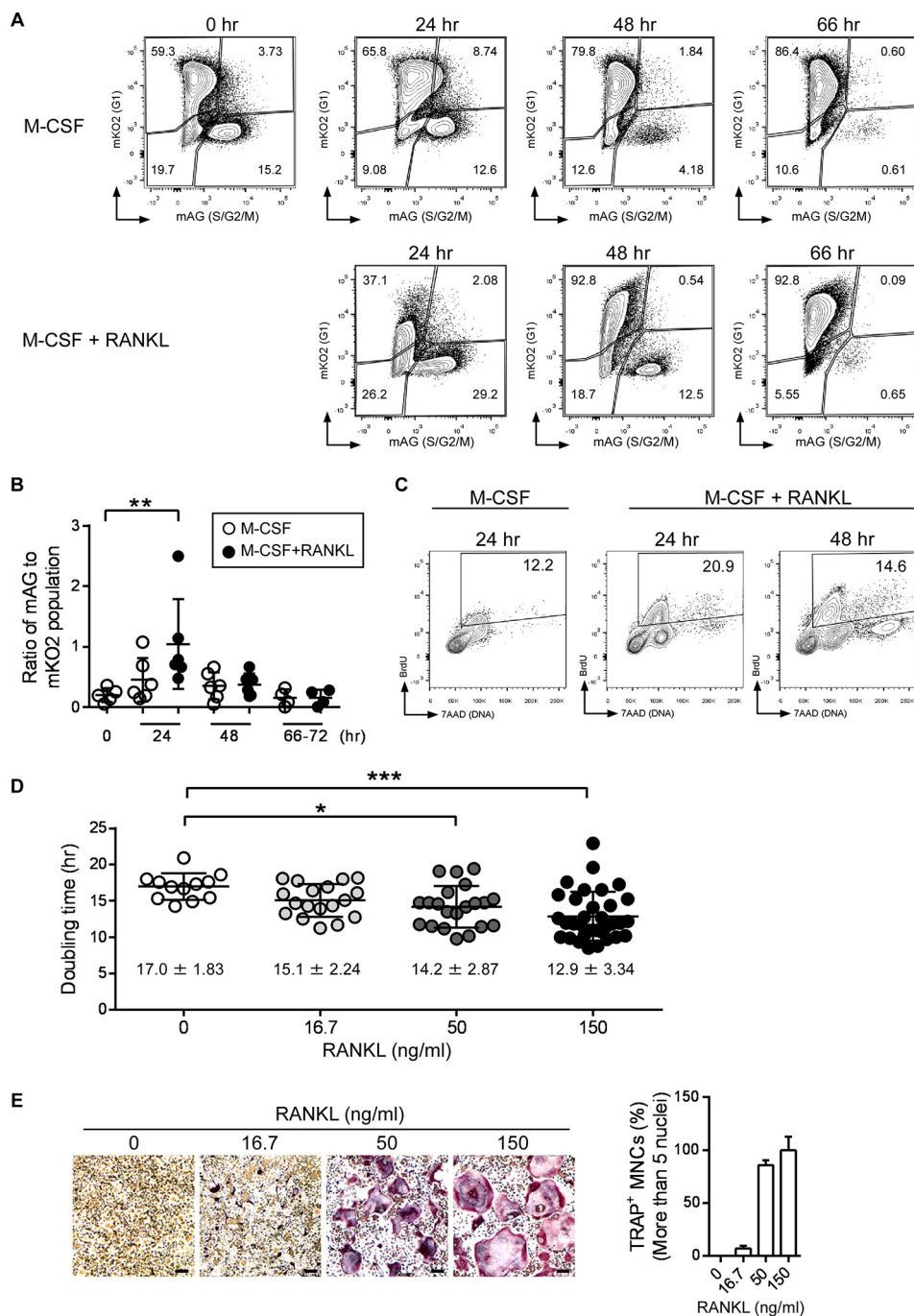


FIGURE 1. RANKL stimulation increases basal cell proliferation. *A*, flow cytometry analysis of dTg-BMMs during osteoclast differentiation. dTg-BMMs were cultured with M-CSF (60 ng/ml) in the presence or absence of RANKL (150 ng/ml) for the indicated times. Cells were harvested at the indicated times, and cells positive for red (mKO2) or green (mAG) fluorescence were detected by flow cytometry. Results are representative of three to five independent experiments. *B*, ratios of red (mKO2) fluorescence-positive cells to green (mAG) fluorescence-positive cells. Each circle represents the result of an independent flow cytometry experiment. Bars indicate means ± S.D. *C*, BrdU incorporation assay. WT-BMMs were cultured with M-CSF (60 ng/ml) in the presence or absence of RANKL (150 ng/ml) for the indicated amount of time (in hours). BrdU (10 μM) was added for the last 6 h. Incorporated BrdU was stained with FITC-labeled anti-BrdU antibody. DNA was stained with 7-AAD and analyzed by flow cytometry. Numbers indicate the percentages of S phase cells. Results are representative of three independent experiments. *D*, doubling time of dTg-BMMs during osteoclast differentiation. dTg-BMMs were cultured with M-CSF (60 ng/ml) in the presence of the indicated dose of RANKL (ng/ml) for 48 h. Each circle represents the result of a cell. Bars indicate means ± S.D. *, $p < 0.05$; ***, $p < 0.001$. *E*, *in vitro* osteoclast differentiation. dTg-BMMs were cultured with M-CSF (60 ng/ml) in the presence of the indicated dose of RANKL (ng/ml) for 96 h. Percentages of multinucleated cells containing more than five nuclei are shown. Scale bars, 100 μm.

Using time-lapse imaging, we measured the doubling time of dTg-BMMs cultured with M-CSF in the presence or absence of RANKL for 48 h. RANKL significantly reduced doubling time in a dose-dependent manner (Fig. 1D), along with increasing formation of multinucleated osteoclasts (Fig. 1E). These results

support the idea that RANKL stimulation increases the basal proliferation of dTg-BMMs.

RANKL Stimulation Induces Polyploid Cells Not Only by Cell Fusion but Also by Incomplete Cytokinesis—We next performed ploidy analysis during osteoclast formation. dTg-BMMs were

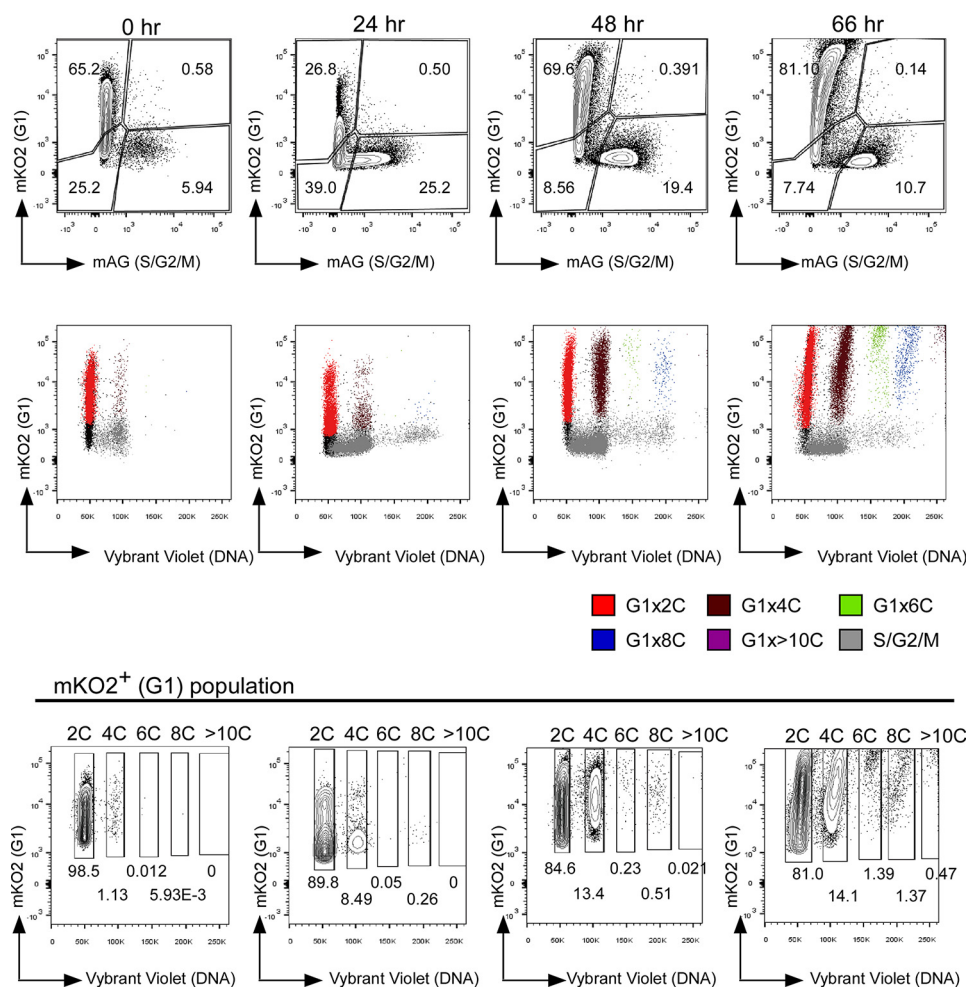


FIGURE 2. RANKL induces polyploid cells. Ploidy analysis of dTg-BMMs during osteoclast differentiation. dTg-BMMs were cultured with M-CSF (60 ng/ml) and RANKL (150 ng/ml) for the indicated times. Cells were harvested at the indicated times, stained with DNA staining dye (Vybrant DyeCycle Violet), and examined by flow cytometry. *Top row* shows flow cytometry results of dTg-BMMs cultured with RANKL for the indicated times. *Middle row* shows flow cytometry results of red fluorescence (mKO2) versus Vybrant DyeCycle Violet. *Bottom row* provides quantitation of the flow cytometry results shown above. 2C, 4C, 6C, 8C, and >10C cells are gated. Numbers indicate the percentages of red (mKO2) positive cells in each bin. Results are representative of three independent experiments.

stimulated with RANKL for the indicated times in the presence of M-CSF, and ploidy was analyzed by flow cytometry (Fig. 2). As expected, stimulation with RANKL induced generation of polyploid cells (red fluorescence-positive 4C, 6C, 8C, and >10C) (Fig. 2). Among these polyploid cells, 4C and 8C cells were detected first after RANKL stimulation for 24 h (Fig. 2). By contrast, 6C cells were not detected until 48 h after the onset of RANKL stimulation, and 6C cells were less common than 8C cells (Fig. 2 and Table 1).

To examine how these polyploid cells were generated, we performed time-lapse imaging. In these experiments, dTg-BMMs were stimulated by RANKL for various times (1–16 h) in the presence of M-CSF, and then cell cycle progression and polyploidization were observed by time-lapse imaging. Regardless of the period of RANKL stimulation, almost all cells were mononucleated at the beginning of imaging. No cell fusion was observed within 24 h, but fusion was observed at and after 36 h of RANKL stimulation (average time of the beginning of fusion was 50.5 ± 5.63 h; Fig. 3A). The majority of cells that went through cell fusion were red fluorescence-positive mononucleated cells (Fig. 3B and Table 2), and the resultant fused cells rarely went through mitosis (Table 2). Instead, they continued

TABLE 1

Percentage of diploid and polyploid cells among mKO2⁺ cells

Each row represents the result of an independent flow cytometry experiment.

	2C	4C	6C	8C	>10C
Monocytes	98.32	1.00			
Monocytes	97.93	1.20	0.03		
Monocytes	94.25	3.89			
Monocytes	92.42	5.36	0.04	0.08	
Monocytes	93.39	4.11	0.09	0.09	
OC (day2)	84.77	12.94	0.25	0.49	0.02
OC (day2)	83.17	13.04	0.17	0.73	
OC (day2)	77.27	16.02	0.66	1.27	
OC (day3)	77.92	13.10	1.32	1.47	1.61
OC (day3)	81.81	13.80	0.59	1.13	

to undergo cell fusion, and finally became large multinucleated osteoclast-like cells with red nuclei. These observations suggested that 4C and 8C cells detected after 24 h of RANKL stimulation were not fusion products. Unexpectedly, incomplete cytokinesis was observed during this period (Fig. 4A and [supplemental Movie 1](#)). The incomplete cytokinesis resulted in formation of 4C binucleated cells (Fig. 4A). Some of these cells re-entered mitosis but failed to complete cytokinesis, resulting in formation of binucleated 8C cells (Fig. 4A). Consistent with

Osteoclast Polyplodization via Incomplete Cytokinesis

this, after RANKL stimulation for 24 h, flow cytometric analysis detected S/G₂/M phase cells between the 4C and 8C peaks (Fig. 2), consistent with the observation that some of the tetraploid cells re-entered the cell cycle. Together, these observations suggested that 4C and 8C cells detected at 24 h after RANKL stimulation resulted from incomplete cytokinesis.

Cells That Undergo Incomplete Cytokinesis Have the Potential for Cell Fusion—Because generation of polyploidy by incomplete cytokinesis has been observed in certain pathological contexts (25, 26), we speculated that cells that undergo incomplete cytokinesis might merely be abnormal, rather than critical intermediates in the formation of mature osteoclasts. To address this issue, we continued time-lapse imaging to trace the fates of cells that underwent incomplete cytokinesis. Cell-tracking analysis revealed that binucleated cells generated by incomplete cytokinesis could undergo cell fusion (Fig. 5A and supplemental Movie 2). Indeed, 11% of fused cells had previously undergone incomplete cytokinesis (Table 2). These results indicated that such cells had the potential to undergo cell fusion during RANKL-induced osteoclast formation.

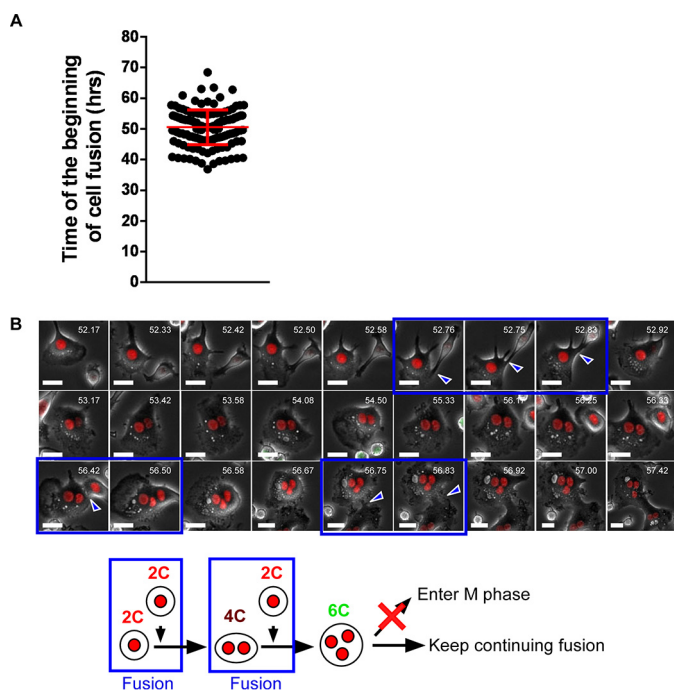


FIGURE 3. Cell fusion occurs at and after 36 h of RANKL stimulation. *A*, time of initiation of cell fusion after RANKL stimulation. Images were taken every 5 min, and the time required for cell fusion was calculated. A total of 145 cells that underwent cell fusion are plotted. *Red bar* indicates means \pm S.D. *B*, representative snapshots of mononucleated cell-cell fusion. Fluorescence and phase-contrast images were taken every 5 min. *Blue arrowheads and boxes* indicate cell fusion. *White numbers* in each image indicates time after RANKL stimulation. *Bottom* schematically depicts the results observed in *B*. *Scale bars*, 20 μ m.

TABLE 2
Fusion summary of osteoclasts

Event	Fusion combination			Total no. (%)
	mKO2 (DN) \times mKO2 (DN)	mKO2 (DN) \times mAG	mAG \times mAG	
Cell fusion	132	12	1	145
Cell fusion involving incomplete cytokinesis	16	0	0	16 (11.0)
Cytokinesis after fusion	0	0	1	1 (0.69)

Some of the binucleated cells generated by incomplete cytokinesis ultimately succeeded in undergoing cytokinesis and formed mononucleated polyploid cells (Fig. 4B and supplemental Movie 3). These mononucleated polyploid cells also had the potential to undergo cell fusion (Fig. 5B and supplemental Movie 4). Notably, \sim 50% of 4C cells sorted from dTg-BMMs cultured with RANKL for 66 h were mononucleated.⁴ These observations strongly suggested that mononucleated cells involved in cell fusion consisted of both 2C and polyploid cells. During time-lapse imaging, target cells often migrated away from the field of view. In this case, the fate of the target cells could not be traced, and consequently those cells were uncaptured. Thus, the observed percentage of cell fusion involving cells that undergo incomplete cytokinesis might represent an underestimate. Collectively, these results revealed that polyploid cells detected after RANKL stimulation for more than 48 h consisted not only of fusion products but also of cells that underwent incomplete cytokinesis.

Characterization of Cells That Undergo Incomplete Cytokinesis—To understand the phenotype of cells that had undergone incomplete cytokinesis, we first examined the expression profiles of integrin β 3, F4/80, and V-type H⁺-ATPase α 3 subunit in RANKL-stimulated BMMs. Integrin β 3 is an important cell adhesion molecule that plays an important role in osteoclast biology (27), and F4/80 is a macrophage marker that is barely expressed on osteoclasts (28). Expression of both integrin β 3 and F4/80 was detected on dTg-BMMs and changed after 48 h of stimulation with RANKL (Fig. 6A). We separated dTg-BMMs into four groups depending on their cell cycle phase and DNA content as follows: (i) mononucleated cells (G₁ \times 2C); (ii) cells in S phase (S); (iii) cells that underwent incomplete cytokinesis or were generated by cell fusion (G₁ \times 4C, G₁ \times 8C), and (iv) cells that underwent incomplete cytokinesis and re-entered S phase (*S (re-enter)*) (Fig. 6B). The expression of integrin β 3 and F4/80 was examined in each of these groups. Flow cytometry analysis revealed that the expression levels of these molecules were approximately the same in all four groups (Fig. 6B), suggesting that the expression of integrin β 3 and F4/80 was not affected by incomplete cytokinesis.

V-type H⁺-ATPase α 3 subunit is a protein complex that mediates H⁺ transport into the resorption lacunae. Lack of α 3 subunit results in severe osteopetrosis due to impaired osteoclast bone-resorbing function (29). BMMs derived from Fucci-mKO2 and α 3-GFP-expressing mice (Fucci-mKO2/ α 3-GFP-BMMs) were cultured with M-CSF and RANKL for the indicated times, and the expression of α 3-GFP was analyzed by flow cytometry. The expression of α 3-GFP gradually increased with time (Fig. 6C) and was detected in diploids (G₁ \times 2C),

⁴ N. Takegahara and Y. Choi, unpublished observations.

Osteoclast Polyplodization via Incomplete Cytokinesis

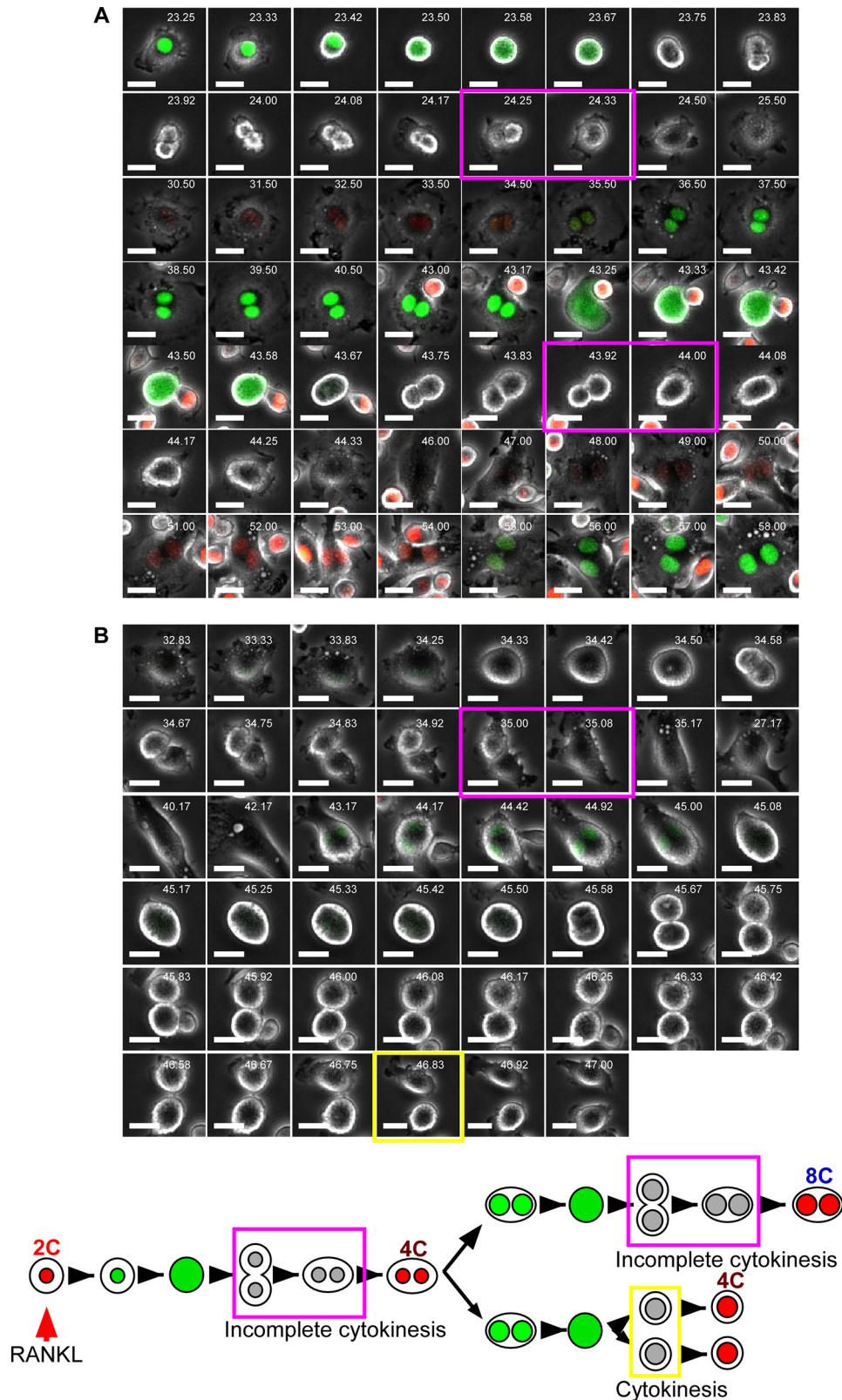


FIGURE 4. RANKL stimulation induces formation of polyploid cells by incomplete cytokinesis. *A*, representative snapshots of dTg-BMMs that underwent incomplete cytokinesis after RANKL stimulation. Fluorescence and phase-contrast images were taken every 5 min. *B*, representative snapshots of dTg-BMMs that underwent cytokinesis after incomplete cytokinesis. *Magenta boxes* indicate incomplete cytokinesis, and the *yellow box* indicates cytokinesis. *White numbers* in each image indicates time after RANKL stimulation. *Scale bars*, 20 μ m. Results are representative of five independent experiments. *Bottom* shows the scheme depicting the results observed in *A* and *B*.

Osteoclast Polyplodization via Incomplete Cytokinesis

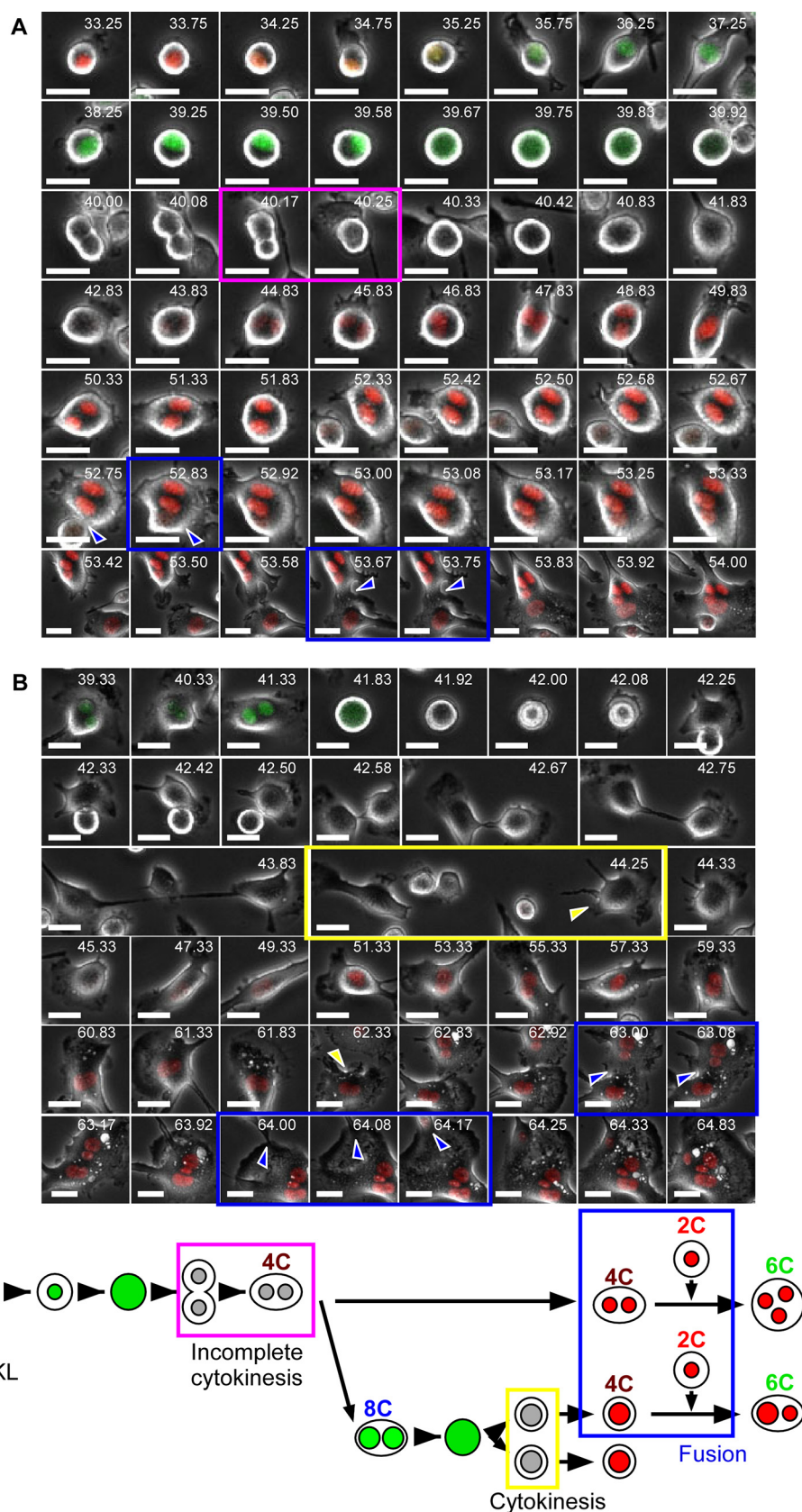


FIGURE 5. **Cells that undergo incomplete cytokinesis have the potential to undergo cell fusion.** *A*, representative snapshots of a binucleated cell that underwent incomplete cytokinesis and subsequently underwent cell fusion. Fluorescence and phase-contrast images were taken every 5 min. *B*, representative snapshots of a mononucleated cell that underwent incomplete cytokinesis and subsequently underwent cell fusion. *Blue arrowheads and blue boxes* indicate cell fusion. The *magenta box* indicates incomplete cytokinesis, and the *yellow box* indicates cytokinesis. *White numbers* in each image indicate the time after RANKL stimulation. *Scale bars*, 20 μm . Results are representative of five independent experiments. *Bottom* shows the scheme depicting the results observed in *A* and *B*.

Osteoclast Polyplodization via Incomplete Cytokinesis

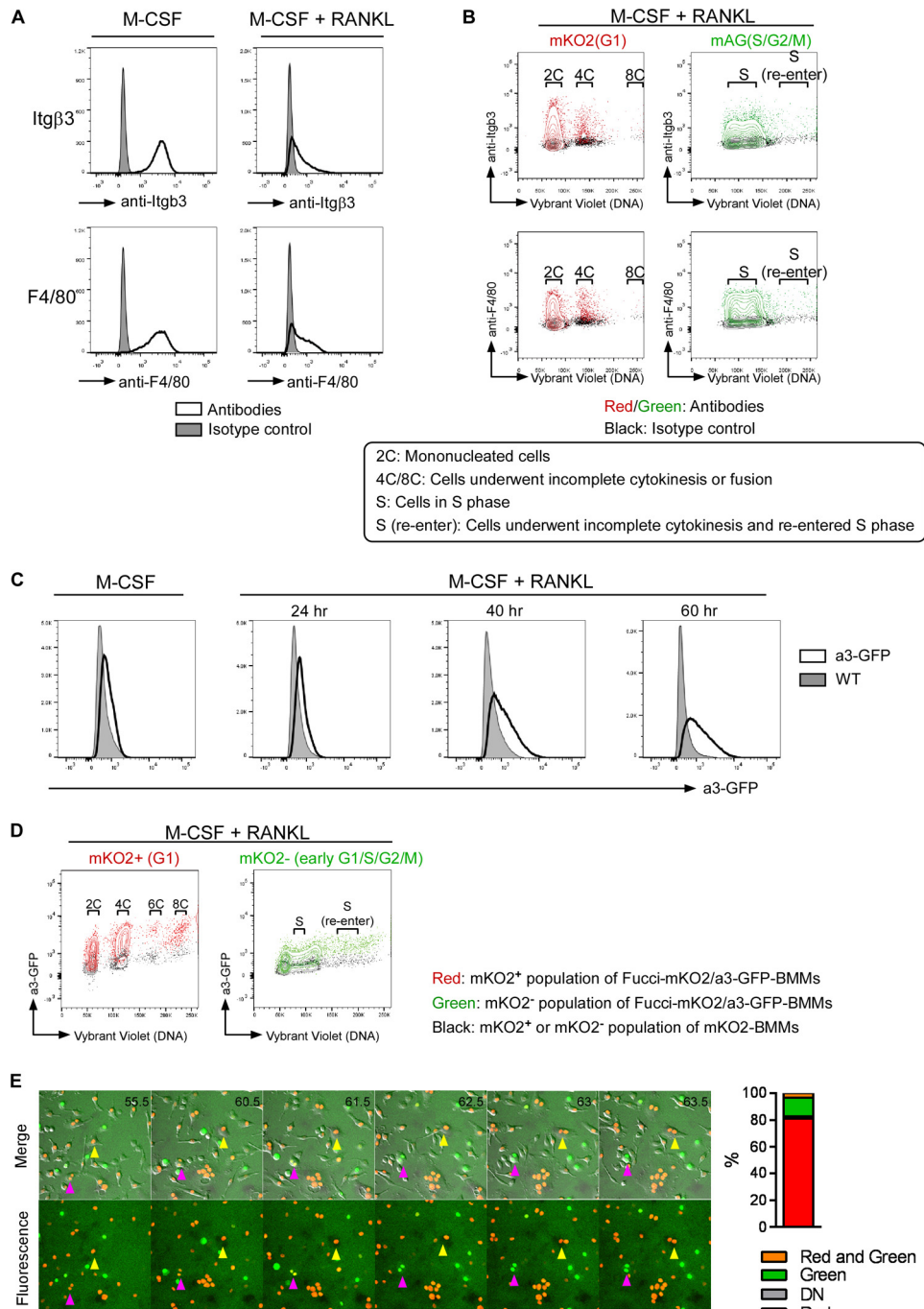


FIGURE 6. Characterization of cells that undergo incomplete cytokinesis. *A*, dTg-BMMs were cultured with M-CSF (60 ng/ml) in the presence or absence of RANKL (150 ng/ml). After 48 h of culture, cells were harvested and stained with anti-integrin $\beta 3$ or anti-F4/80. The levels of these molecules were determined by flow cytometry. *B*, dTg-BMMs described in *C* were divided into four groups depending on their cell cycle state and DNA contents as follows: mononucleated cells ($G_1 \times 2C$); cells in S phase (S); cells that underwent incomplete cytokinesis or were generated by cell fusion ($G_1 \times 4C$, $G_1 \times 8C$); and cells that underwent incomplete cytokinesis and re-entered S phase (S (re-enter)). *C*, expression profiles of a3-GFP in Fucci-mKO2/a3-GFP-BMMs cultured with M-CSF (60 ng/ml) in the presence or absence of RANKL (150 ng/ml) for the indicated times. *D*, Fucci-mKO2/a3-GFP-BMMs cultured with M-CSF (60 ng/ml) and RANKL (150 ng/ml) for 60 h were divided into diploids, polyploids, and cells in S phase (S (re-enter)) depending on their cell cycle state and DNA contents. *E*, left, representative snapshots of dTg-BMMs cultured on FITC gelatin-coated culture dishes. dTg-BMMs cultured on FITC gelatin-coated dishes for 24 h were observed. Fluorescence and bright field images were taken every 30 min. Yellow arrowheads indicate a cell in G_1 phase that underwent cell fusion, and magenta arrowheads indicate a cell that underwent incomplete cytokinesis and re-entered S phase (S (re-enter)). Black numbers in each image indicate time after RANKL stimulation (hours). Right, percentage of cells that degraded FITC gelatin during the imaging.

polyploids ($G_1 \times 4C$, $G_1 \times 6C$, and $G_1 \times 8C$), and cells that underwent incomplete cytokinesis and re-entered S phase (S (re-enter)) (Fig. 6D). These results suggested that the expression of a3-GFP was not affected by incomplete cytokinesis.

We next examined resorption activities of cells that had undergone incomplete cytokinesis. dTg-BMMs were cultured on FITC-labeled gelatin-coated dishes in the presence of M-CSF and RANKL for 24 h, and then time-lapse imaging was

Osteoclast Polyplodization via Incomplete Cytokinesis

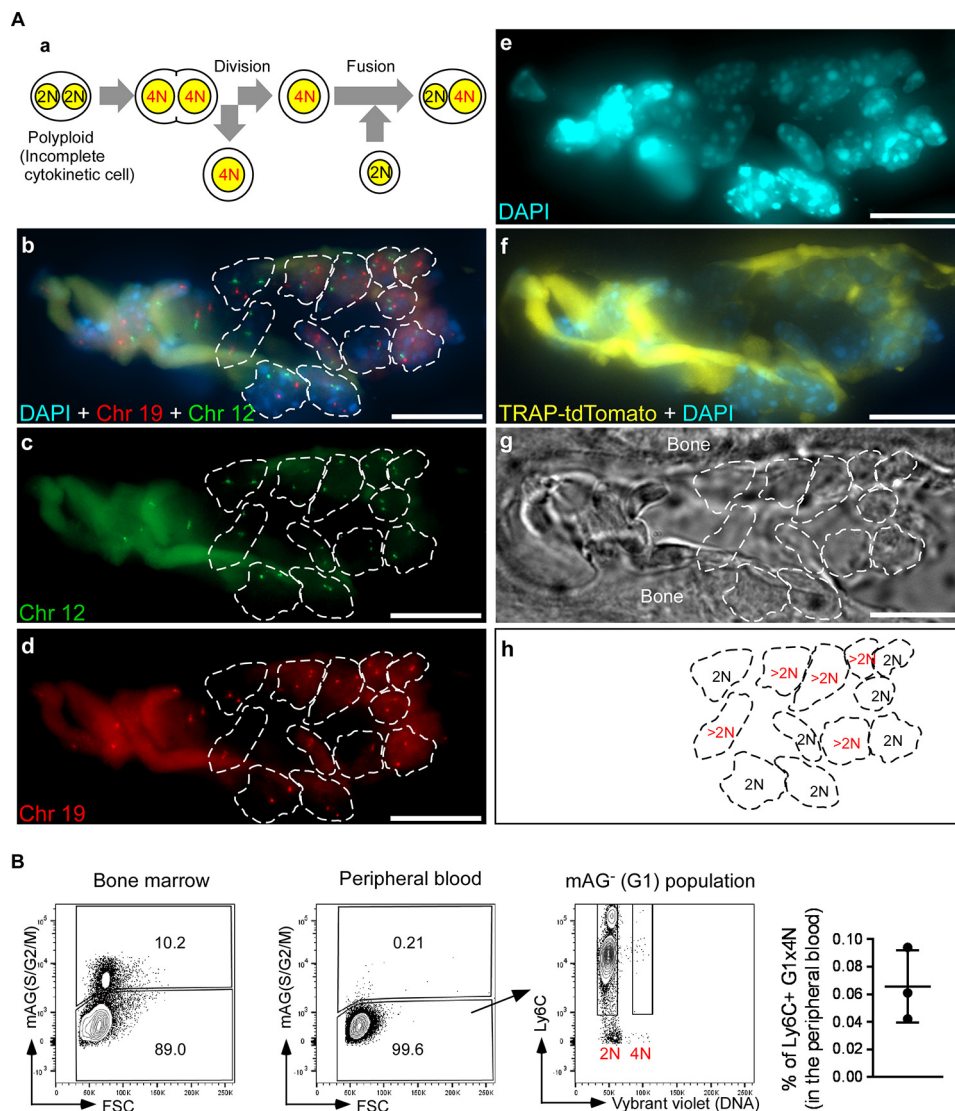


FIGURE 7. Diploid and polyplod nuclei are observed in osteoclasts *in vivo*. *A*, representative micrographs of fluorescence *in situ* hybridization (FISH). *A*, *panel a*, scheme depicting generation of polyploidy by cell fusion of diploid cells and cells that undergo incomplete cytokinesis. *Panel b*, bone sections of TRAP promoter-tdTomato transgenic mice were hybridized with probes for chromosome 12 (green) and chromosome 19 (red). Nuclei were stained with DAPI (blue). *Panel c*, micrograph of FISH with a probe for chromosome 12 in the same visual field as *panel b*. *Panel d*, micrograph of FISH with a probe for chromosome 19 in the same visual field as *panel b*. *Panel e*, micrograph of nuclei (DAPI: blue) in the same visual field as *panel b*. *Panel f*, merged micrograph of TRAP-tdTomato cells (yellow) and nuclei (DAPI: blue) in the same visual field as *panel b*. *Panel g*, a bright field micrograph of the same view filed shown in *panel b*. *Panel h*, outlines of osteoclast precursors *in vivo*. Peripheral blood cells or bone marrow cells were prepared from Fucci-mAG mice and examined the cell cycle phase, expression of Ly6C, and DNA content. The graph shows percentage of Ly6C⁺ G₁ × 4C cells in the peripheral blood. Each circle represents the result of a mouse. Bars indicate means ± S.D.

performed. Resorption activity can be observed as degradation of the gelatin. Majority of cells that degraded FITC gelatin were in red (81.0%; Fig. 6E). In contrast, green⁺ binucleated cells (*i.e.* the cells that underwent incomplete cytokinesis and re-entered S phase) barely degraded FITC gelatin (Fig. 6E and supplemental movie 5). These results suggested that cells that had undergone incomplete cytokinesis and re-entered S phase had lower resorption capacity than cells in G₁ phase.

*Cells That Undergo Incomplete Cytokinesis Are Involved in Formation of Multinucleated Osteoclasts *In Vivo**—To determine whether incomplete cytokinesis plays a physiologically relevant role in development of multinucleated osteoclasts, we performed two experiments. First, we examined the ploidy of osteoclasts *in vivo*. Fusion of cells that had previously under-

gone incomplete cytokinesis would result in some osteoclasts exhibiting nuclear polyploidy (*i.e.* containing nuclei with more than the diploid complement of chromosomes) (Fig. 7A, *panel a*). In transgenic mice in which tdTomato, a red fluorescent protein, is expressed under the control of the TRAP promoter, osteoclasts are labeled with tdTomato. We analyzed the ploidy profiles of osteoclasts in the long bone of TRAP-tdTomato transgenic mice by fluorescence *in situ* hybridization. In tdTomato⁺ osteoclasts, some nuclei had the diploid complement of chromosomes (2N), whereas others had more than the diploid complement (>2N) (Fig. 7A, *panels b–h*).

Next, we examined the existence of osteoclast precursors that had undergone incomplete cytokinesis *in vivo* by flow cytometry. Because Ly6C is reported as one of markers of oste-

oclast precursors (30), and osteoclast precursors are circulating in the periphery (31), we tried to detect Ly6C⁺ G₁ × 4C cells in the peripheral blood. In the peripheral blood of Fucci-mAG transgenic mice, green⁺ cells were barely detected. In green⁻ (G₁ phase) cells, Ly6C⁺ 4C cells were detected (average percentage was 0.07 ± 0.03%; Fig. 7B). These results indicated that almost all circulating cells were in G₁ phase under physiological conditions, and G₁ × 4C osteoclast precursors could be detected in the periphery. Although we cannot exclude the possibility that the cells were binucleated fusion products, this observation may support in some part the idea that incomplete cytokinesis occurs *in vivo*. These results suggested that fusion of cells that undergo incomplete cytokinesis occurs *in vivo* and that incomplete cytokinesis contributes to physiological development of multinucleated osteoclasts.

Fusion of Cells That Undergo Incomplete Cytokinesis Occurs during Formation of Osteoclasts but Not MGCs—Next, we examined the involvement of incomplete cytokinesis in formation of MGCs (32, 33). MGCs are formed by cell fusion of macrophages in response to foreign bodies at the site of implantation, and they can be formed *in vitro* from monocytes following stimulation with combinations of cytokines such as IL-4 and IL-3. Various common molecules (*e.g.* DC-STAMP, OC-STAMP, and Atp6v0d2) are required for polyploidization of both osteoclasts and MGCs (13, 34, 35), suggesting that MGCs might become multinuclear via a process similar to that of osteoclasts. Stimulation with IL-4 plus IL-3 induced formation of polyploid cells but only rarely induced cell proliferation (Fig. 8A). This observation was confirmed by BrdU incorporation assays (Fig. 8B). Consistent with these observations, neither incomplete cytokinesis nor cell fusion involving incomplete cytokinesis was observed (Table 3). These results suggested that fusion of cells that undergo incomplete cytokinesis may be involved in formation of RANKL-induced osteoclasts but not MGCs.

Cell cycle progression seems to be required for formation of multinucleated osteoclasts but not MGCs. To address this point, we examined the effect of blocking cell cycle on multinucleation of osteoclasts and MGCs. Treatment with aphidicolin, an inhibitor of nuclear DNA replication that blocks the cell cycle at early S phase, drastically increased green cell proportion in RANKL-stimulated osteoclasts, but only slightly in IL-4 + IL-3-stimulated MGCs (Fig. 9A), indicating that aphidicolin induced S phase arrest in osteoclasts but not in MGCs. In addition, treatment with aphidicolin significantly inhibited formation of multinucleated osteoclasts, but not MGCs (Fig. 9B). These results suggested that RANKL but not IL-4 plus IL-3 promoted cell cycle progression and supported the idea that cell cycle progression is necessary for formation of multinucleated osteoclasts but not MGCs. Therefore, although osteoclasts and MGCs are generated from the same lineage of progenitors and require common molecules to become multinuclear, the mechanisms underlying the formation of these distinct types of multinucleated cells are likely to be different.

RANKL-induced Akt Activation Controls Incomplete Cytokinesis during Osteoclast Development—To understand the molecular mechanism by which incomplete cytokinesis is controlled during RANKL-induced osteoclast multinucleation, we

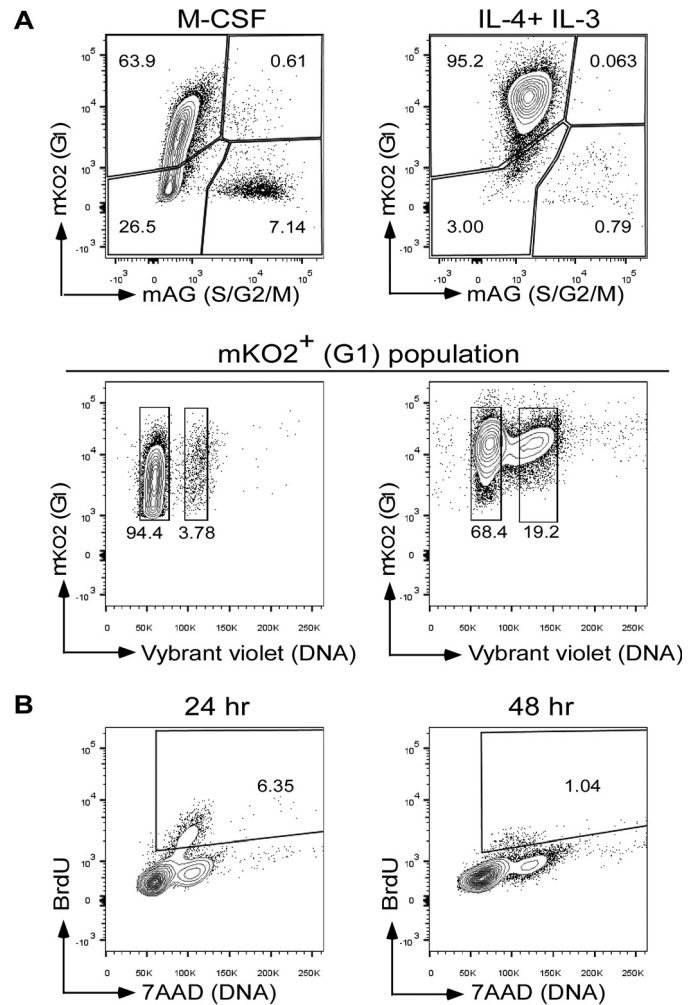


FIGURE 8. Flow cytometry analysis of dTg-BMMs during MGC formation. *A, top*, dTg-BMMs were cultured with IL-4 (100 ng/ml) plus IL-3 (100 ng/ml) for 48 h to induce formation of MGCs. Cells were harvested, and cells positive for red (mKO2) or green (mAG) fluorescence were detected by flow cytometry. *Bottom*, ploidy analysis of dTg-BMMs during MGC differentiation. dTg-BMMs cultured with IL-4 (100 ng/ml) and IL-3 (100 ng/ml) for 48 h were harvested, stained with DNA staining dye (Vybrant DyeCycle Violet), and examined by flow cytometry. 2C and 4C cells of red (mKO2) fluorescence-positive cells are gated. Numbers indicate the percentages of red (mKO2)-positive cells in each bin. Results are representative of three independent experiments. *B*, BrdU incorporation assay. WT-BMMs were cultured with IL-4 (100 ng/ml) plus IL-3 (100 ng/ml) for the indicated amount of time (in hours). BrdU (10 μM) was added for the last 6 h. Cells were harvested, and incorporated BrdU was stained with FITC-labeled anti-BrdU antibody. DNA was stained with 7-AAD and analyzed by flow cytometry. Numbers indicate the percentages of S phase cells. Results are representative of three independent experiments.

first examined a small GTPase, Rho, which plays a role in cytokinesis by regulating the contractile ring (36, 37). Treatment with Y27632, a selective inhibitor of Rho-associated protein kinase (ROCK), a downstream target of Rho, neither inhibited nor promoted generation of multinucleated osteoclasts (Fig. 10A). These results suggested that Rho is not an important factor in RANKL-induced osteoclast multinucleation.

We next searched for signal molecules whose activation is induced in osteoclasts but not in MGCs. We examined phosphorylation of MAPKs (p38, ERK, and JNK) and Akt and degradation of IκBα. We found that phosphorylation of Akt and degradation of IκBα were induced in RANKL-stimulated osteoclasts more than twice as much as those in monocytes but

Osteoclast Polyploidization via Incomplete Cytokinesis

TABLE 3

Fusion summary of MGCs

Event	Fusion combination			Total no. (%)
	mKO2 (DN) × mKO2 (DN)	mKO2 (DN) × mAG	mAG × mAG	
Cell fusion	64	12	0	76
Cell fusion involving incomplete cytokinesis	0	0	0	0 (0.0)
Cytokinesis after fusion	2	1	0	3 (3.95)

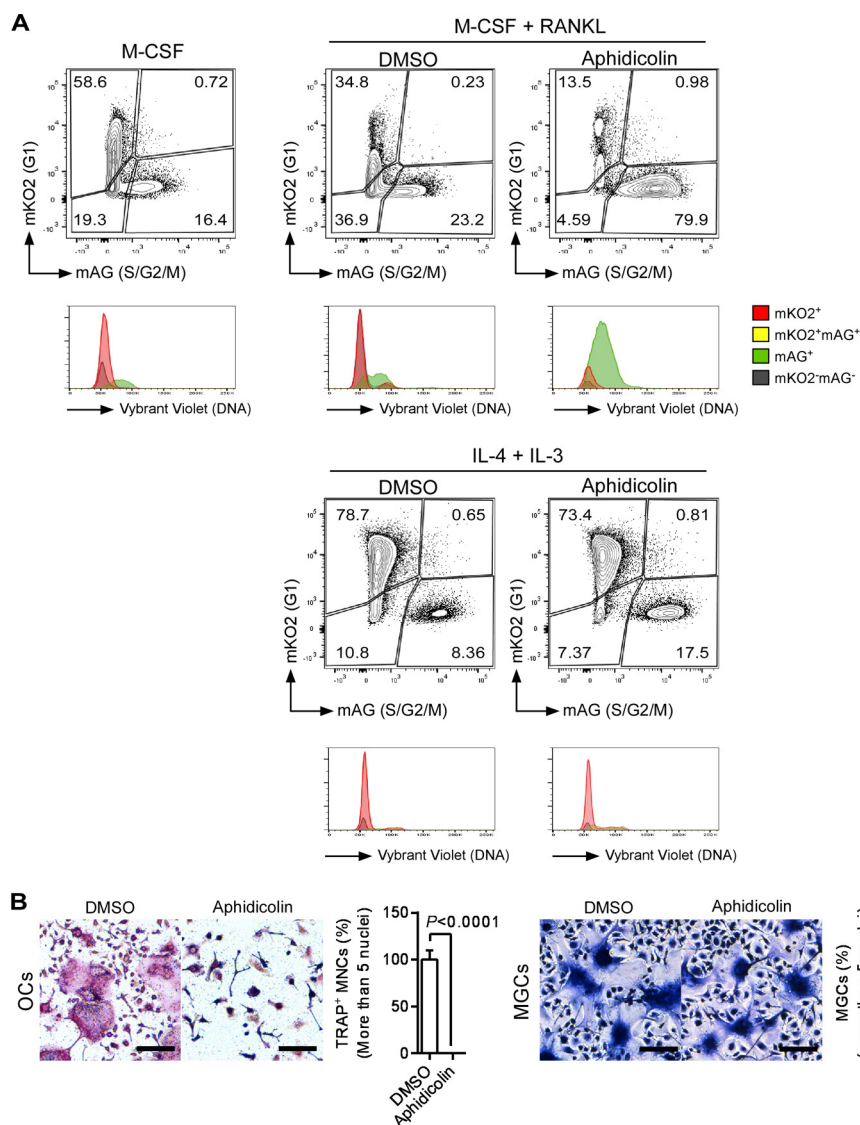


FIGURE 9. Flow cytometry analysis of dTg-BMMs after treatment with cell cycle inhibitors. A, dTg-BMMs were stimulated with M-CSF (60 ng/ml) and RANKL (150 ng/ml) or IL-4 (100 ng/ml) plus IL-3 (100 ng/ml) in the presence of aphidicolin (500 nM) or DMSO for 24 h. Cells were harvested and analyzed by flow cytometry. Results are shown in contour plots and histograms. B, TRAP staining (osteoclasts) or Giemsa staining (MGCs) is shown. Percentage of multinucleated cells containing more than five nuclei. Data represent means \pm S.D. Results are representative of three independent experiments. OC, osteoclasts; ns, not significant.

were only slightly induced in IL-4 + IL-3-stimulated MGCs (Fig. 10B). Both Akt and NF- κ B are involved in osteoclast formation (38–40). Consistent with previous reports, blocking Akt activation by treatment with Akt inhibitor VIII or blocking NF- κ B activation by treatment with SN50 prevented RANKL-induced formation of multinucleated osteoclasts (Fig. 10, C and D). Blocking NF- κ B activation also inhibited MGC formation (Fig. 10D). However, blocking of Akt activation did not inhibit IL-4 + IL-3-induced MGC formation (Fig. 10C).

To better understand the role of Akt and NF- κ B in multinucleation and incomplete cytokinesis of osteoclasts, we performed time-lapse imaging. In these experiments, dTg-BMMs were stimulated with RANKL in the presence or absence of inhibitors for 1 h, and then cell cycle progression and polyploidization were observed. RANKL induced incomplete cytokinesis in a dose-dependent manner (Fig. 11), and the increase in incomplete cytokinesis was significantly inhibited when Akt activation was blocked (89.3% lower than in control osteoclasts

Osteoclast Polyplodization via Incomplete Cytokinesis

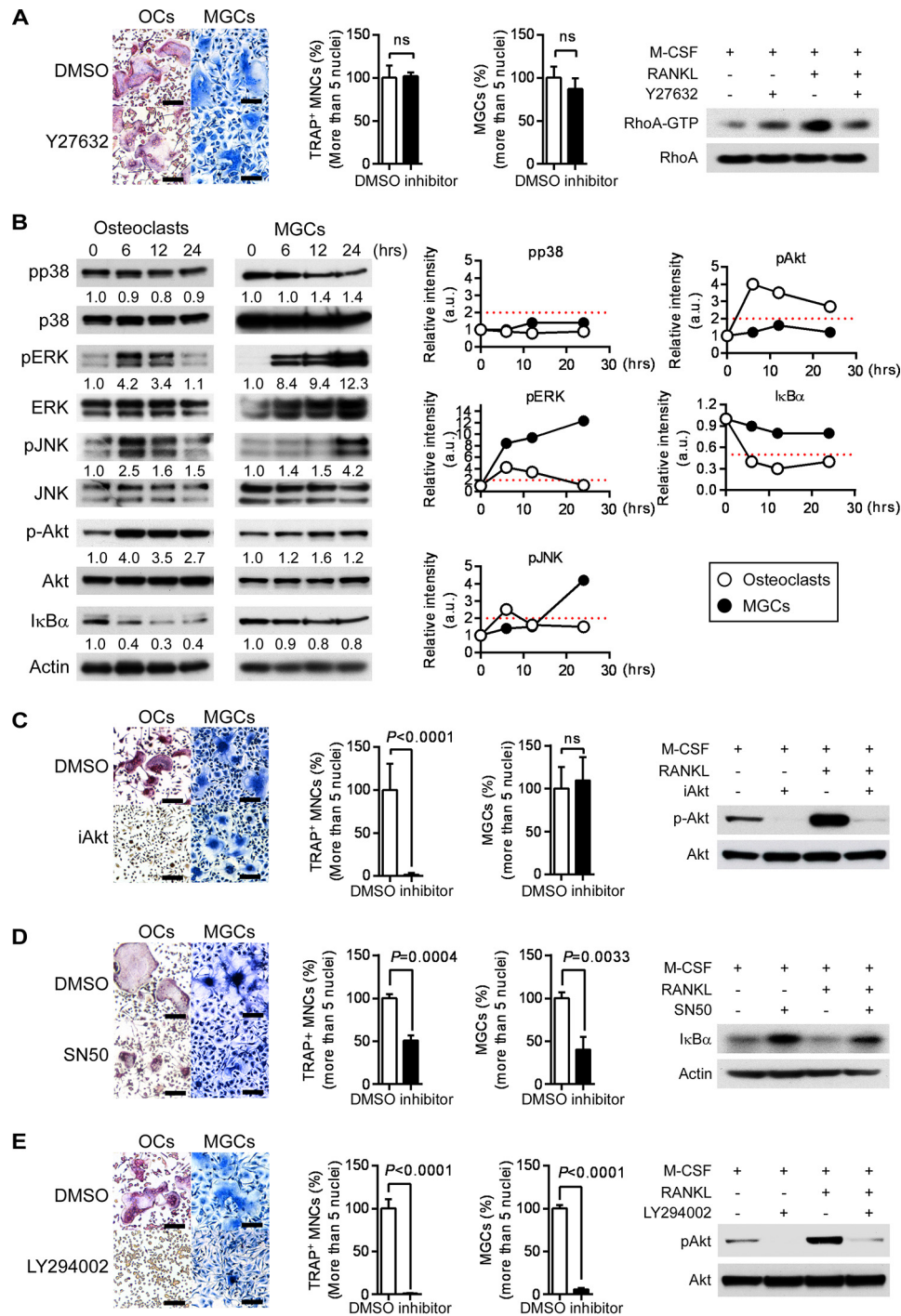


FIGURE 10. Searching signaling molecule(s) that regulates osteoclast multinucleation. *A, left*, *in vitro* differentiation of osteoclasts or MGCs from BMMs treated with Y27632 (10 μ M) or DMSO. TRAP staining (osteoclasts) or Giemsa staining (MGCs) is shown. Percentage of multinucleated cells containing more than five nuclei. Data represent means \pm S.D. *Right*, BMMs were pretreated for 2 h with Y27632 or DMSO and then stimulated with or without RANKL in the presence of M-CSF for 6 h. Cell lysates were used for RhoA activation assay and immunoblotted with the indicated antibodies. *B*, phosphorylation of MAPKs and Akt and degradation of $\text{IkB}\alpha$ during osteoclast or MGC differentiation. Lysates from BMMs stimulated with M-CSF (60 ng/ml) plus RANKL (150 ng/ml) (osteoclasts) or IL-4 (100 ng/ml) plus IL-3 (100 ng/ml) (MGCs) for the indicated times were immunoblotted with the indicated antibodies. Relative band intensities are shown below the Western blot (*left*) and plotted (*right*). *Red dashed lines* indicate relative signal intensities twice as much as those in monocytes (0 h). *a.u.*, arbitrary unit. *C–E, left*, *in vitro* differentiation of osteoclasts or MGCs from BMMs treated with Akt inhibitor VIII (iAkt, 5 μ M) (*C*), SN50 (50 μ g/ml) (*D*), LY294002 or DMSO (5 μ M) (*E*). TRAP staining (osteoclasts) or Giemsa staining (MGCs) is shown. Percentage of multinucleated cells containing more than five nuclei. Data represent means \pm S.D. *Right*, BMMs were pretreated for 2 h with Akt inhibitor VIII, SN50, LY294002, or DMSO and then stimulated with or without RANKL in the presence of M-CSF for 6 h. Cell lysates were immunoblotted with the indicated antibodies. Percentage of multinucleated cells containing more than five nuclei. Data represent means \pm S.D. Results are representative of three independent experiments. OC, osteoclasts; *ns*, not significant.

treated with 150 ng/ml RANKL; Fig. 11). Akt inhibitor VIII also decreased entry to mitotic phase by half (53.4% lower than in control osteoclasts treated with 150 ng/ml RANKL; Fig. 11),

suggesting that Akt may play a role in regulating both incomplete cytokinesis and cell cycle progression during osteoclast differentiation. Inhibition of NF- κ B activation by SN50

Osteoclast Polyploidization via Incomplete Cytokinesis

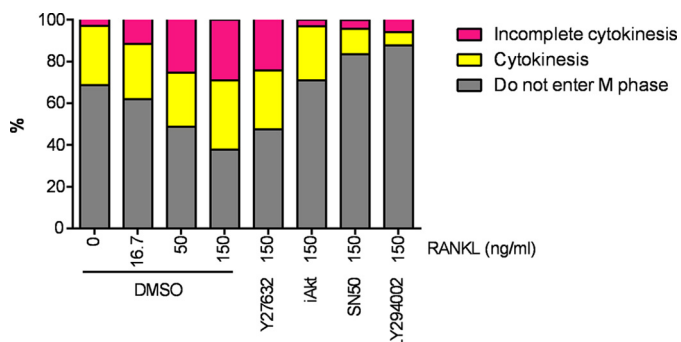


FIGURE 11. Akt regulates incomplete cytokinesis and formation of multinucleated osteoclasts. A, percentage of cells that went through incomplete cytokinesis (magenta) or cytokinesis (yellow). dTg-BMMs were cultured with M-CSF (60 ng/ml) and RANKL in the presence of the indicated reagents. Cells that did not enter mitotic phase are shown in gray. Data shown as percentage of cells pooled from two independent experiments.

decreased not only incomplete cytokinesis (85.2% lower than in control osteoclasts treated with 150 ng/ml RANKL; Fig. 11) but also entry to mitotic phase (73.5% lower than in control osteoclasts treated with 150 ng/ml RANKL; Fig. 11), suggesting that NF- κ B signaling pathway is involved in cell cycle progression in osteoclasts. Considering that SN50 inhibited multinucleation of MGCs (Fig. 10D), which were generated by incomplete cytokinesis-independent fusion (Figs. 8 and 9), it is plausible that NF- κ B signaling pathway plays roles not only in cell cycle progression but also in fusion. Taken together, these results suggest that Akt-dependent RANKL-induced incomplete cytokinesis is involved in the formation of polyploid osteoclasts.

Discussion

Osteoclasts require polyploidization to acquire sufficient bone-resorbing activity. Using Fucci-expressing BMMs, we were able to distinguish polyploid cells from S/G₂/M phase cells by flow cytometry. In combination with time-lapse imaging analysis, we showed that the polyploidization of osteoclasts is due to not only cell fusion, but also incomplete cytokinesis. In addition, we demonstrated nuclear polyploidy of osteoclasts *in vivo*. Although incomplete cytokinesis has been extensively studied in pathological contexts, its role in physiological contexts remains unclear. Our findings reveal the importance of incomplete cytokinesis in the formation of polyploid osteoclasts, a normal physiological process.

Using inhibitors, we sought to identify signaling molecules that control incomplete cytokinesis during osteoclast polyploidization. Blocking ROCK neither inhibited nor promoted osteoclast multinucleation and had no effect on cytokinesis or incomplete cytokinesis during osteoclast formation (Figs. 10A and 11). Although the Rho signaling pathway regulates cytokinesis by driving actin and myosin, our observations suggested that it may not play a major role in either cytokinesis/incomplete cytokinesis or cell fusion in osteoclast polyploidization. Blocking NF- κ B decreased formation of osteoclasts and MGCs (Fig. 10, B and D). In addition, blocking NF- κ B activation inhibited not only incomplete cytokinesis but also cell cycle progression (Fig. 11). These results suggested that NF- κ B may not be specifically involved in regulation of incomplete cytokinesis.

We identified Akt as a key molecule involved in the control of incomplete cytokinesis during osteoclast polyploidization.

Notably in this regard, Akt plays a role in the formation of tetraploid vascular smooth endothelial cells and hepatocytes by regulating incomplete cytokinesis (41, 42). Our results suggest that Akt-mediated incomplete cytokinesis is a general program involved in the formation of polyploidy. We cannot exclude the possibility that Akt also plays a role in the cell fusion process. Future work should further explore the role of Akt in incomplete cytokinesis and cell fusion. Blocking Akt activation also attenuated entry into mitosis (Fig. 11). Indeed, Akt is involved in cell cycle regulation (43). These observations suggest that Akt plays multiple roles during osteoclastogenesis, including regulation of both incomplete cytokinesis and cell cycle progression. Of note, stimulation with RANKL, but not IL-4 plus IL-3, promoted cell cycle progression (Fig. 9A), and blocking the RANKL-induced cell cycle progression inhibited formation of multinucleated osteoclasts (Fig. 9B). These results reinforce the idea that mitotic entry and cell cycle progression are important for generation of multinucleated osteoclasts.

Akt is an important downstream effector of PI3K, which is also involved in osteoclast formation (44), suggesting that the PI3K-Akt signaling pathway plays a role in osteoclast multinucleation. However, blocking of PI3K activation by treatment with the selective PI3K inhibitor LY294002 significantly inhibited not only incomplete cytokinesis (79.5% lower than in control-treated osteoclasts) but also cytokinesis (81.3% lower than in control-treated osteoclasts) (Fig. 11). In addition, blocking PI3K inhibited formation of both RANKL-induced multinucleated osteoclasts and IL-4 + IL-3-induced MGCs (Fig. 10E). In addition to Akt, PI3K also regulates Vav3, phospholipase C γ 2, and Grb2 activation (45). Hence, it is plausible that PI3K regulates a number of biological events, including incomplete cytokinesis. Further investigation will be required to understand the contribution of the PI3K-Akt pathway to regulation of RANKL-induced incomplete cytokinesis. We also examined the involvement of molecules previously determined to play a role in cell fusion, such as DC-STAMP, in blocking antibody experiments (anti-DC-STAMP mAb, clone 1A2); however, we did not see a specific effect on incomplete cytokinesis (data not shown). Future studies should attempt to clarify the involvement of fusion-related molecules in incomplete cytokinesis.

The molecular mechanism that selectively regulates incomplete cytokinesis during polyploidization of osteoclasts remains unclear. We observed Akt-regulated incomplete cytokinesis in RANKL-induced osteoclasts but not in IL-4 + IL-3-induced MGCs. These results suggest that the binding of RANKL to receptor activator of nuclear factor- κ B, the receptor for RANKL, triggers signaling pathways that selectively regulate incomplete cytokinesis. Further studies will be required to determine the molecular mechanisms underlying regulation of incomplete cytokinesis by Akt during osteoclastogenesis.

We observed a low incidence (11%) of cell fusion involving incomplete cytokinesis during formation of multinucleated osteoclasts *in vitro* (Table 2), implying that there are at least two types of polyploid osteoclasts as follows: one generated by diploid cells (canonical cell fusion) and the other generated by diploid cells and cells that undergo incomplete cytokinesis (atypical cell fusion) (Fig. 12). We did not try to observe cell fusion following incomplete cytokinesis (atypical cell fusion) *in*

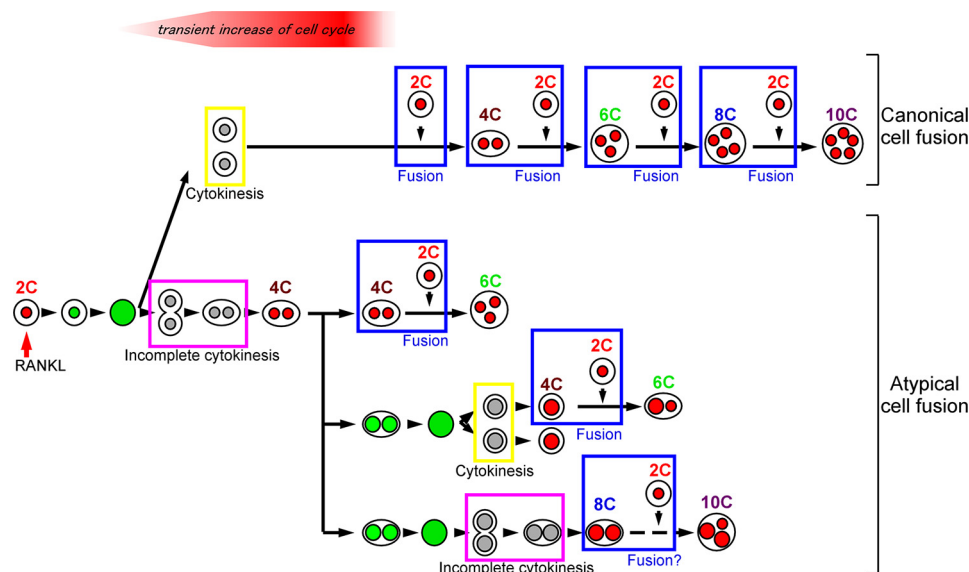


FIGURE 12. **Schematic model depicting the process of osteoclast polyploidization.** RANKL stimulation induces a transient increase in cell cycle activity, leading to cell fusion (canonical cell fusion). Along with the transient increase in cell cycle progression, some cells undergo incomplete cytokinesis. The resultant cells have the potential to undergo cell fusion and are involved in the formation of polyploid osteoclasts (atypical cell fusion).

in vivo because the phenomenon takes more than a day, surpassing the current time limit for intravital imaging. Instead, we used fluorescence *in situ* hybridization to reveal that osteoclasts have nuclei with more than the diploid complement of chromosomes ($>2N$). In addition, we found circulating osteoclast precursors ($Ly6C^+$ cells) that were $G_1 \times 4C$. These results suggested that cells that increase ploidy via cell cycle-dependent mechanisms are involved in the formation of multinucleated osteoclasts *in vivo*. However, we cannot exclude the possibilities that the nuclear polyploidy might also be caused by nuclear fusion, and $Ly6C^+ G_1 \times 4C$ cells were merely fusion products. Further studies will be required to clarify this issue.

The proportion of multinucleated osteoclasts generated by atypical cell fusion *in vivo*, as well as the functional differences between osteoclasts generated by canonical cell fusion and osteoclasts generated by atypical cell fusion, still remains unclear. FITC gelatin resorption assay showed that the cells that underwent incomplete cytokinesis and re-entered S phase (green⁺ binucleated cells) barely degraded FITC gelatin (Fig. 6E). These observations suggested that osteoclasts generated by atypical cell fusion might have relatively lower resorption activity than that by canonical cell fusion. However, it cannot be excluded that the difference of the resorption activity between cells in G_1 phase and cells in S phase merely reflected the difference of their cell cycle phase. To address these issues, it will be necessary to identify specific markers expressed on cells that undergo incomplete cytokinesis.

What is the physiological significance of polyploid nuclei within a cell? This phenomenon may be just one aspect of the phenotype of terminally differentiated cells, or a consequence of stress response that preserves cell function. Alternatively, polyploid nuclei may create genetic diversity, which could promote better adaptation to chronic injury or stress (2, 46, 47). Very little is known regarding the physiological function of the polyploid state, largely due to technical limitations (*e.g.* there currently exist no methods for converting a tissue composed of

polyploid cells into a tissue of the same size composed of diploid cells). A full understanding of the mechanisms of polyploidization is necessarily to reveal the physiological significance of osteoclast polyploidization via cell fusion and incomplete cytokinesis.

Author Contributions—N. T. and Y. C. designed the study and wrote the paper. N. T., H. K., and H. M. performed and analyzed the experiments. A. S., A. M., M. T., O. K., and M. I. provided reagents and data analysis. All authors reviewed the results and approved the final version of the manuscript.

Acknowledgments—We thank Dr. Matt Walsh for critical discussion and reading the manuscript. We also thank to the Cell and Developmental Biology Microscopy Core, Perelman School of Medicine, University of Pennsylvania, for technical assistance with microscopy.

References

- Otto, S. P. (2007) The evolutionary consequences of polyploidy. *Cell* **131**, 452–462
- Pandit, S. K., Westendorp, B., and de Bruin, A. (2013) Physiological significance of polyploidization in mammalian cells. *Trends Cell Biol.* **23**, 556–566
- Sakaue-Sawano, A., Hoshida, T., Yo, M., Takahashi, R., Ohtawa, K., Arai, T., Takahashi, E., Noda, S., Miyoshi, H., and Miyawaki, A. (2013) Visualizing developmentally programmed endoreplication in mammals using ubiquitin oscillators. *Development* **140**, 4624–4632
- Edgar, B. A., Zielke, N., and Gutierrez, C. (2014) Endocycles: a recurrent evolutionary innovation for post-mitotic cell growth. *Nat. Rev. Mol. Cell Biol.* **15**, 197–210
- Lee, H. O., Davidson, J. M., and Duronio, R. J. (2009) Endoreplication: polyploidy with purpose. *Genes Dev.* **23**, 2461–2477
- Machlus, K. R., and Italiano, J. E., Jr. (2013) The incredible journey: from megakaryocyte development to platelet formation. *J. Cell Biol.* **201**, 785–796
- Gentric, G., Desdouets, C., and Celton-Morizur, S. (2012) Hepatocytes polyploidization and cell cycle control in liver physiopathology. *Int. J. Hepatol.* **2012**, 282430
- Gentric, G., Celton-Morizur, S., and Desdouets, C. (2012) Polyploidy and

- liver proliferation. *Clin. Res. Hepatol. Gastroenterol.* **36**, 29–34
9. Aguilar, P. S., Baylies, M. K., Fleissner, A., Helming, L., Inoue, N., Podbilewicz, B., Wang, H., and Wong, M. (2013) Genetic basis of cell-cell fusion mechanisms. *Trends Genet.* **29**, 427–437
 10. Srinivas, B. P., Woo, J., Leong, W. Y., and Roy, S. (2007) A conserved molecular pathway mediates myoblast fusion in insects and vertebrates. *Nat. Genet.* **39**, 781–786
 11. Teitelbaum, S. L. (2000) Bone resorption by osteoclasts. *Science* **289**, 1504–1508
 12. Walsh, M. C., Kim, N., Kadono, Y., Rho, J., Lee, S. Y., Lorenzo, J., and Choi, Y. (2006) Osteoimmunology: interplay between the immune system and bone metabolism. *Annu. Rev. Immunol.* **24**, 33–63
 13. Yagi, M., Miyamoto, T., Sawatani, Y., Iwamoto, K., Hosogane, N., Fujita, N., Morita, K., Ninomiya, K., Suzuki, T., Miyamoto, K., Oike, Y., Takeya, M., Toyama, Y., and Suda, T. (2005) DC-STAMP is essential for cell-cell fusion in osteoclasts and foreign body giant cells. *J. Exp. Med.* **202**, 345–351
 14. Oren-Suissa, M., and Podbilewicz, B. (2007) Cell fusion during development. *Trends Cell Biol.* **17**, 537–546
 15. Mizoguchi, T., Muto, A., Udagawa, N., Arai, A., Yamashita, T., Hosoya, A., Ninomiya, T., Nakamura, H., Yamamoto, Y., Kinugawa, S., Nakamura, M., Nakamichi, Y., Kobayashi, Y., Nagasawa, S., Oda, K., et al. (2009) Identification of cell cycle-arrested quiescent osteoclast precursors *in vivo*. *J. Cell Biol.* **184**, 541–554
 16. Meiyanto, E., Hoshijima, M., Ogawa, T., Ishida, N., and Takeya, T. (2001) Osteoclast differentiation factor modulates cell cycle machinery and causes a delay in S phase progression in RAW264 cells. *Biochem. Biophys. Res. Commun.* **282**, 278–283
 17. Sankar, U., Patel, K., Rosol, T. J., and Ostrowski, M. C. (2004) RANKL coordinates cell cycle withdrawal and differentiation in osteoclasts through the cyclin-dependent kinase inhibitors p27KIP1 and p21CIP1. *J. Bone Miner. Res.* **19**, 1339–1348
 18. Kim, N. S., Kim, H. J., Koo, B. K., Kwon, M. C., Kim, Y. W., Cho, Y., Yokota, Y., Penninger, J. M., and Kong, Y. Y. (2006) Receptor activator of NF- κ B ligand regulates the proliferation of mammary epithelial cells via Id2. *Mol. Cell Biol.* **26**, 1002–1013
 19. Aiba, Y., Kometani, K., Hamadate, M., Moriyama, S., Sakaue-Sawano, A., Tomura, M., Luche, H., Fehling, H. J., Casellas, R., Kanagawa, O., Miyawaki, A., and Kurosaki, T. (2010) Preferential localization of IgG memory B cells adjacent to contracted germinal centers. *Proc. Natl. Acad. Sci. U.S.A.* **107**, 12192–12197
 20. Tomura, M., Sakaue-Sawano, A., Mori, Y., Takase-Utsugi, M., Hata, A., Ohtawa, K., Kanagawa, O., and Miyawaki, A. (2013) Contrasting quiescent G₀ phase with mitotic cell cycling in the mouse immune system. *PLOS ONE* **8**, e73801
 21. Sakaue-Sawano, A., Kurokawa, H., Morimura, T., Hanyu, A., Hama, H., Osawa, H., Kashiwagi, S., Fukami, K., Miyata, T., Miyoshi, H., Imamura, T., Ogawa, M., Masai, H., and Miyawaki, A. (2008) Visualizing spatiotemporal dynamics of multicellular cell cycle progression. *Cell* **132**, 487–498
 22. Abe, T., Sakaue-Sawano, A., Kiyonari, H., Shioi, G., Inoue, K., Horiuchi, T., Nakao, K., Miyawaki, A., Aizawa, S., and Fujimori, T. (2013) Visualization of cell cycle in mouse embryos with Fucci2 reporter directed by Rosa26 promoter. *Development* **140**, 237–246
 23. Kikuta, J., Wada, Y., Kowada, T., Wang, Z., Sun-Wada, G. H., Nishiyama, I., Mizukami, S., Maiya, N., Yasuda, H., Kumanogoh, A., Kikuchi, K., Germain, R. N., and Ishii, M. (2013) Dynamic visualization of RANKL and Th17-mediated osteoclast function. *J. Clin. Invest.* **123**, 866–873
 24. Yamaguchi, H., Yoshida, S., Muroi, E., Yoshida, N., Kawamura, M., Kouchi, Z., Nakamura, Y., Sakai, R., and Fukami, K. (2011) Phosphoinositide 3-kinase signaling pathway mediated by p110 α regulates invadopodia formation. *J. Cell Biol.* **193**, 1275–1288
 25. Storchova, Z., and Pellman, D. (2004) From polyploidy to aneuploidy, genome instability and cancer. *Nat. Rev. Mol. Cell Biol.* **5**, 45–54
 26. Comai, L. (2005) The advantages and disadvantages of being polyploid. *Nat. Rev. Genet.* **6**, 836–846
 27. Teitelbaum, S. L., and Ross, F. P. (2003) Genetic regulation of osteoclast development and function. *Nat. Rev. Genet.* **4**, 638–649
 28. Takahashi, N., Udagawa, N., Tanaka, S., Murakami, H., Owan, I., Tamura, T., and Suda, T. (1994) Postmitotic osteoclast precursors are mononuclear cells which express macrophage-associated phenotypes. *Dev. Biol.* **163**, 212–221
 29. Scimeca, J. C., Franchi, A., Trojani, C., Parrinello, H., Grosgeorge, J., Robert, C., Jaillon, O., Poirier, C., Gaudray, P., and Carle, G. F. (2000) The gene encoding the mouse homologue of the human osteoclast-specific 116-kDa V-ATPase subunit bears a deletion in osteosclerotic (oc/oc) mutants. *Bone* **26**, 207–213
 30. Jacome-Galarza, C. E., Lee, S. K., Lorenzo, J. A., and Aguila, H. L. (2013) Identification, characterization, and isolation of a common progenitor for osteoclasts, macrophages, and dendritic cells from murine bone marrow and periphery. *J. Bone Miner. Res.* **28**, 1203–1213
 31. Ishii, M., Egen, J. G., Klauschen, F., Meier-Schellersheim, M., Saeki, Y., Vacher, J., Proia, R. L., and Germain, R. N. (2009) Sphingosine-1-phosphate mobilizes osteoclast precursors and regulates bone homeostasis. *Nature* **458**, 524–528
 32. Brodbeck, W. G., and Anderson, J. M. (2009) Giant cell formation and function. *Curr. Opin. Hematol.* **16**, 53–57
 33. Vignery, A. (2005) Macrophage fusion: are somatic and cancer cells possible partners? *Trends Cell Biol.* **15**, 188–193
 34. Miyamoto, H., Suzuki, T., Miyauchi, Y., Iwasaki, R., Kobayashi, T., Sato, Y., Miyamoto, K., Hoshi, H., Hashimoto, K., Yoshida, S., Hao, W., Mori, T., Kanagawa, H., Katsuyama, E., Fujie, A., et al. (2012) Osteoclast stimulatory transmembrane protein and dendritic cell-specific transmembrane protein cooperatively modulate cell-cell fusion to form osteoclasts and foreign body giant cells. *J. Bone Miner. Res.* **27**, 1289–1297
 35. Lee, S. H., Rho, J., Jeong, D., Sul, J. Y., Kim, T., Kim, N., Kang, J. S., Miyamoto, T., Suda, T., Lee, S. K., Pignolo, R. J., Koczon-Jaremko, B., Lorenzo, J., and Choi, Y. (2006) v-ATPase V0 subunit d2-deficient mice exhibit impaired osteoclast fusion and increased bone formation. *Nat. Med.* **12**, 1403–1409
 36. Glotzer, M. (2005) The molecular requirements for cytokinesis. *Science* **307**, 1735–1739
 37. Etienne-Manneville, S., and Hall, A. (2002) Rho GTPases in cell biology. *Nature* **420**, 629–635
 38. Moon, J. B., Kim, J. H., Kim, K., Youn, B. U., Ko, A., Lee, S. Y., and Kim, N. (2012) Akt induces osteoclast differentiation through regulating the GSK3 β /NFATc1 signaling cascade. *J. Immunol.* **188**, 163–169
 39. Greenblatt, M. B., Park, K. H., Oh, H., Kim, J. M., Shin, D. Y., Lee, J. M., Lee, J. W., Singh, A., Lee, K. Y., Hu, D., Xiao, C., Charles, J. F., Penninger, J. M., Lotinun, S., Baron, R., et al. (2015) CHMP5 controls bone turnover rates by dampening NF- κ B activity in osteoclasts. *J. Exp. Med.* **212**, 1283–1301
 40. Abu-Amer, Y., Darwech, I., and Otero, J. (2008) Role of the NF- κ B axis in immune modulation of osteoclasts and bone loss. *Autoimmunity* **41**, 204–211
 41. Celson-Morizur, S., Merlen, G., Couton, D., Margall-Ducos, G., and Desdouets, C. (2009) The insulin/Akt pathway controls a specific cell division program that leads to generation of binucleated tetraploid liver cells in rodents. *J. Clin. Invest.* **119**, 1880–1887
 42. Hixon, M. L., Muro-Cacho, C., Wagner, M. W., Obejero-Paz, C., Millie, E., Fujio, Y., Kureishi, Y., Hassold, T., Walsh, K., and Gualberto, A. (2000) Akt1/PKB upregulation leads to vascular smooth muscle cell hypertrophy and polyploidization. *J. Clin. Invest.* **106**, 1011–1020
 43. Gonzalez, E., and McGraw, T. E. (2009) The Akt kinases: isoform specificity in metabolism and cancer. *Cell Cycle* **8**, 2502–2508
 44. Oikawa, T., Oyama, M., Kozuka-Hata, H., Uehara, S., Udagawa, N., Saya, H., and Matsuo, K. (2012) Tks5-dependent formation of circumferential podosomes/invadopodia mediates cell-cell fusion. *J. Cell Biol.* **197**, 553–568
 45. Peng, Q., Malhotra, S., Torchia, J. A., Kerr, W. G., Coggeshall, K. M., and Humphrey, M. B. (2010) TREM2- and DAP12-dependent activation of PI3K requires DAP10 and is inhibited by SHIP1. *Sci. Signal.* **3**, ra38
 46. Leervers, S. J., and McNeill, H. (2005) Controlling the size of organs and organisms. *Curr. Opin. Cell Biol.* **17**, 604–609
 47. Fox, D. T., and Duronio, R. J. (2013) Endoreplication and polyploidy: insights into development and disease. *Development* **140**, 3–12